

UNSTEADY BOUNDARY LAYER TRANSITION ON THE DSA-9A ROTOR BLADE AIRFOIL

K. Richter*¹, S. Koch¹, A. Goertler¹, B. Lütke², C. C. Wolf¹, and A. Benkel³

¹German Aerospace Center (DLR), Institute of Aerodynamics and Flow Technology

²German Aerospace Center (DLR), Institute of Aeroelasticity

³German-Dutch Wind Tunnels (DNW)

Bunsenstrasse 10, 37073 Göttingen, Germany

Abstract

The unsteady boundary layer transition on the pitching helicopter main rotor blade airfoil DSA-9A was experimentally investigated by the use of hot film anemometry and unsteady pressure measurements. The unsteady flow characteristics on the upper and the lower side of the airfoil were analyzed for steady test cases and dynamic cases with sinusoidal pitching motion in attached flow conditions at $M = 0.30$ and $Re = 1.8 \times 10^6$. The paper discusses the unsteady transition characteristics in detail and presents the influence of the pitching frequency on the unsteady transition. The results indicate that a large transition hysteresis exists on both sides of the airfoil, and that the hysteresis is much larger than can be explained by the unsteadiness in lift. Significant transition zones exist on the airfoil with sizes of up to 55% chord. The frequency influence is seen in an increase in the hysteresis and in a reduction of the size of the transition zone with increasing frequency.

NOMENCLATURE

α Angle of attack, deg

α_{50} Angle of attack at 50% intermittency, deg

α_{end} Angle of attack at the end of transition, deg

α_{onset} Angle of attack at transition onset, deg

σ_U Standard deviation of voltage, V

c Chord, m

c_L Lift coefficient

c_P Pressure coefficient

f Frequency, Hz

k Reduced frequency, $k = \frac{\pi f c}{V_\infty}$

l Length of the transition region, m

M Mach number

N Number of samples

Re Reynolds number

s Skewness

T Period, s

t Time, s

U_i Voltage, V

\bar{U} Voltage mean, V

V_∞ Freestream velocity, m/s

x Coordinate in streamwise direction, m

$(x/c)_{onset}$ Dimensionless coordinate of transition onset

1 INTRODUCTION

Modern helicopters are developed to offer excellent aerodynamic performance in a variety of flight conditions. Low power consumption is essential and all major rotorcraft components are designed to have low drag. As the main rotor makes an important contribution to the overall power consumption of the helicopter, modern rotors are optimized to have significant portions of laminar flow on the blades to ensure low drag. Therefore, the laminar/turbulent boundary layer transition plays an important role in the aerodynamics of rotors and rotor blade airfoils, and the transition characteristics have become an inherent part of the airfoil design. State-of-the-art design methodologies try to take the dynamic performance of the oscillating airfoil into account. However, due to a lack of detailed knowledge of

*Corresponding author. Email: kai.richter@dlr.de

the unsteady transition on oscillating rotor blade airfoils and due to the unavailability of reliable unsteady transition prediction tools, the steady transition characteristics of the static airfoil are still used in the design. Potential benefits of taking the unsteady characteristics into account cannot be employed.

Currently the only way to obtain information about the unsteady transition behavior on rotor blades and rotor blade airfoils is wind tunnel testing. The main measurement technique established for unsteady transition detection is the hot film anemometry. Since transition measurements are complex, only few investigations have been undertaken with respect to the dynamic transition characteristics. Very few results were published for rotating blades or rotors with cyclic blade motion: Sémézis & Beaumier [1] measured the unsteady transition on the isolated 7A/7AD model rotor in two radial stations $r/R = 0.70$ (OA213 airfoil) and $r/R = 0.90$ (OA209 airfoil) for different forward flight conditions. In each station, ten hot film sensors were coarsely distributed over the upper and lower sides, providing the transition characteristics for these sections during selected conditions. Raffel et al. [2] published transition results measured on a BO105 model rotor as part of the GOAHEAD helicopter configuration, with 40 sensors distributed over four sections at $r/R \in [0.60, 0.80, 0.90, 0.95]$ (all NACA23012mod airfoil). Due to problems in the experiment, the transition behavior could only be evaluated for a few single sensors.

More investigations were undertaken for pitching airfoils. Most of them dealt with the transition on symmetric NACA airfoils (NACA0012, NACA0015) for incompressible flow at low Reynolds numbers [3, 4, 5, 6, 7]. The measurements had high spatial resolution due to large numbers of hot film sensors of up to 140 and revealed the basic hysteresis that occurs between upstroke and downstroke motion, the basic frequency effect, and the basic Reynolds number effect on the transition location. However, since flow over a helicopter rotor blade is compressible and with Reynolds numbers one order of magnitude higher than in these investigations, the findings are rather of qualitative than of quantitative nature for helicopter aerodynamics.

Investigations performed for high Reynolds numbers are limited to the work of Lorber & Carta [8], Chandrasekhara & Wilder [9] and the main authors of this paper, Richter et al. [10, 11]. Lorber & Carta [8] measured the unsteady transition on the upper side of a finite-span wing using the SSC-A09 rotor blade airfoil with 16 sensors coarsely distributed over three sections, and discussed the upstroke/downstroke hysteresis, the effects of Mach number, model sweep angle, and pitch rate. Chandrasekhara & Wilder [9] performed measurements on a NACA0012 airfoil with 148 sensors in one section, discussing the effects of pitch rate and Mach number. Surprisingly, the data shows no upstroke/downstroke hysteresis. Richter et al. [10, 11] measured transition on the EDI-M109 rotor blade airfoil with 40 sensors in one section. In contrast to the work of the other researchers, who describe the transition location by a



Figure 1: DSA-9A airfoil model in the Transonic Wind Tunnel Goettingen.

single point only, Richter et al. resolve the transitional zone by separating the beginning and the end of the transition zone, and the point of maximum RMS (50% intermittency). With this approach the hysteresis and the effects of pitching amplitude, mean angle of attack and Mach number are discussed for the upper side transition behavior. Since the analysis of the hot film sensor signals was complicated and time consuming, previous publications are typically limited to few test cases, and the number of test cases generally reduced when the number of sensors increased.

This paper presents results of a wind tunnel test studying the unsteady transition on the upper and the lower sides of a helicopter rotor blade airfoil at flight-relevant Reynolds numbers performed in the DLR-project STELAR. With the aid of a new automated transition detection method applied to hot film data, the analysis of a large number of sensors was possible for various test cases. This enabled the detailed investigation of the transition characteristics on both sides of the airfoil and of the influence of the pitching frequency on the transition characteristics.

2 EXPERIMENTAL SETUP

A two-dimensional model of the rotor blade airfoil DSA-9A was used. The carbon-fiber composite model had a chord, c , of 300 mm, a span of 997 mm, and a maximum thickness of 9% chord. The model was mounted horizontally in the $1\text{ m} \times 1\text{ m}$ adaptive-wall test section of the Transonic Wind Tunnel Göttingen (DNW-TWG), as shown in Fig. 1, and was driven via drive shafts through the side-walls attached at the quarter-chord location. The adaptive test section has a flexible ceiling and floor which were statically adapted based on the mean angle of attack of the model to minimize the wall interferences. Hydraulic motors, located outside the test section, drove the model from both sides. The model was fitted with 50 Kulite® XCQ-093 unsteady pressure sensors in a single section. The sensors were situated to have a maximum discretization error of 1% in the lift and pitching-moment coefficients evaluated from the pressure taps.

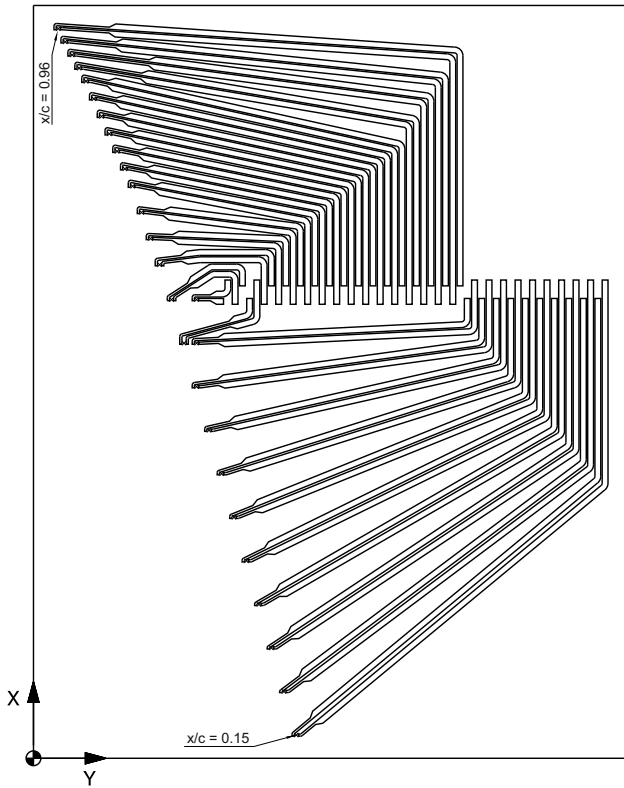
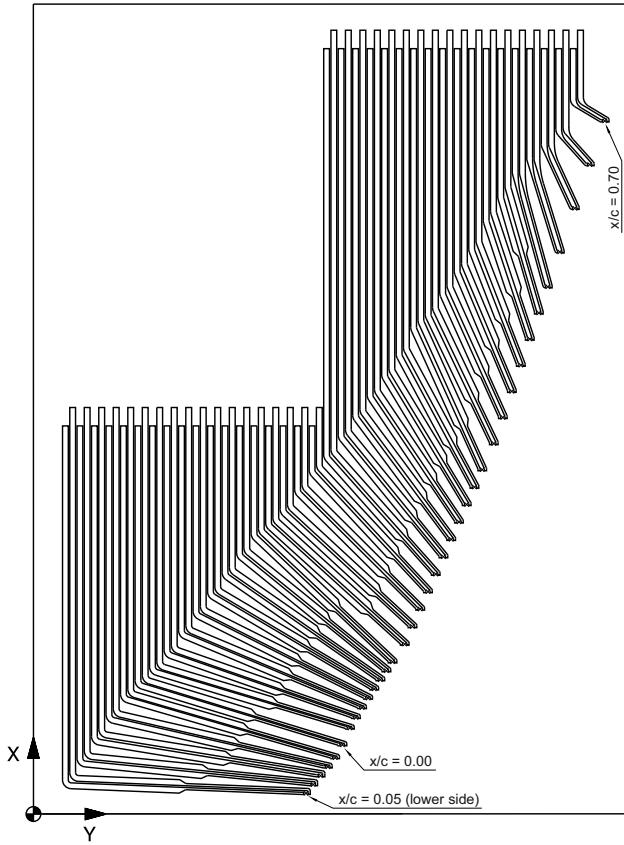


Figure 2: Layout of the top side (top) and bottom side (bottom) hot film sensor arrays

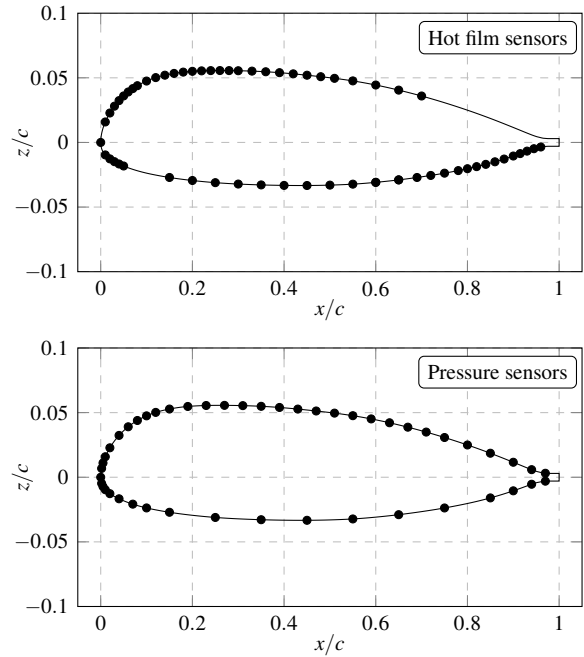


Figure 3: Distribution of hot film sensors and pressure sensors in the DSA-9A cross section

The model was additionally equipped with 61 customized Senflex[®] hot film sensors distributed on two Upilex[®] S polyimide sheets on the upper and lower surfaces of the model. The sensor array layout, the arrangement of the sheets on the model, and the electrical integration were designed to minimize disturbance of the measurements and of the airfoil flow. The layouts of the sensor arrays are shown in Fig. 2. The sensors were placed on a line with an inclination of at least 15° to the main flow direction to reduce the passage of a sensor's wake over other sensors. The upper-surface sheet was wrapped around the model leading edge and contained 36 sensors between $x/c = 0.70$ on the upper surface and $x/c = 0.05$ on the lower surface. The sensors had an increasing spacing starting from $\Delta x/c = 0.01$ around the leading edge and reaching $\Delta x/c = 0.05$ downstream of $x/c = 0.55$. The lower-surface sheet was completely attached to the lower model side and contained 25 sensors between $x/c = 0.15$ and $x/c = 0.96$ with a spacing between $\Delta x/c = 0.015$ and $\Delta x/c = 0.05$. The sheets were glued onto the model in specially-prepared recesses, so that no thickness was added to the model. The electrical wiring was installed inside of the model. Figure 3 shows the distribution of the hot film and pressure sensors in the model cross section. During the measurements, a few hot film sensors failed: $x/c = 0.24$ on the upper side, and $x/c \in [0.20, 0.60, 0.78, 0.80, 0.96]$ on the lower side.

The hot film sensor arrays consisted of nickel sensor elements and copper leads. The sensor elements had a length of 1.4 mm, a width of 0.1 mm and a height of 0.2 μm . The nominal cold resistance was around 6 Ω/mm , resulting in a sensor-element resistance of approximately 9 – 10 Ω . The

copper leads had a width of 2 mm, height of $5.1 \mu\text{m}$, and varying lengths due to the layout of the array. The nominal cold resistance of the leads was around $0.005 \Omega/\text{mm}$, leading to a maximum resistance of the longest lead of approximately 1.1Ω . The resistance ratio of sensor elements to leads was greater than 9.2 for the entire array. The array was operated in constant-temperature mode with an over-heat ratio of 1.3. No calibration was performed since a calibration for unsteady flows is very complicated and the objective of this experiment was to investigate the qualitative time-dependent behavior of the boundary-layer shear stress characteristics and not the quantitative measurement of the shear stress itself. Hot film data was sampled at a rate of approximately $f = 135 \text{ kHz}$ and synchronized with the pressure measurements that were performed with 1024 samples per model pitching period. The pressure data was recorded for 160 pitching periods, whereas the hot film data was recorded only for the first 80 periods due to the huge amount of data.

Measurements were conducted for a steady polar and several dynamic test points at $M = 0.30$ and $Re = 1.8 \times 10^6$. Sinusoidal pitching motions around mean angles of attack of 4° and 5° with amplitudes of 6° and 7° were performed at frequencies $1.1 \text{ Hz} \leq f \leq 6.6 \text{ Hz}$. The conditions of the test points were chosen to have attached flow during the entire motion.

3 TRANSITION DETECTION

The analysis of pitching airfoil hot film data for transition detection is usually based on the manual analysis of the sensor voltage output. Using the phase-averaged (also called ensemble-averaged in some publications) voltage signal of an individual sensor, transition is detected by a visual interpretation of the changes in voltage levels that occur when the flow state changes between laminar and turbulent, as shown by Lee & Basu [6] and Richter et al. [11]. Such interpretation has to be performed by an expert for each sensor of the hot film array, making the analysis of the data rather complicated and very time consuming. This explains why only few test cases were investigated by each research group in the past, and why the number of published test cases usually further reduced when large numbers of sensors were used.

For the transition detection in this work, a new detection method was developed which allows a computer-aided automated detection of the transition location. This method is based on the skewness of the voltage s

$$s = \frac{1}{N} \sum_{i=1}^N \left(\frac{U_i - \bar{U}}{\sigma_U} \right)^3 \quad (1)$$

computed with the sensor voltage U_i , the mean voltage \bar{U} , the standard deviation of the voltage σ_U , and the number of samples N . The skewness describes the degree of asymmetry of the signal around its mean, and can be used to characterize the boundary layer state in the intermittent flow

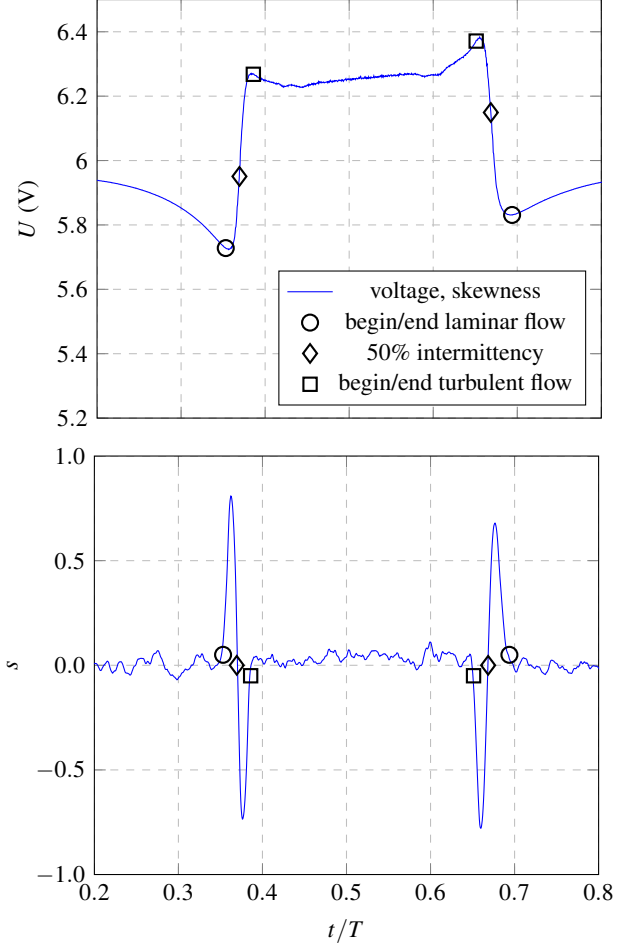


Figure 4: Voltage signal (top) and skewness (bottom) for the sensor at $x/c = 0.07$ on the upper side for $\alpha = 4^\circ \pm 6^\circ$, $f = 6.6 \text{ Hz}$, $M = 0.30$, and $Re = 1.8 \times 10^6$

region as shown by Tiedemann [12] based on the findings of Tetýanko [13]. The skewness of the voltage is computed in a sliding window.

Figure 4 shows the voltage (top) and the skewness (bottom) distributions for a sensor at $x/c = 0.07$ on the upper side of the pitching airfoil as an example. The graphs represent a part of the pitching cycle, with the minimum angle of attack reached at $t/T = 0$ and $t/T = 1$, and the maximum angle of attack at $t/T = 0.5$. For purely laminar flow in $t/T \leq 0.35$ and $t/T \geq 0.69$, and for purely turbulent flow in $0.39 \leq t/T \leq 0.67$, the voltage fluctuations are nearly evenly distributed around the laminar or turbulent mean voltage levels, respectively. The skewness is near zero in both cases. Transition from laminar to turbulent occurs within $0.35 \leq t/T \leq 0.39$. In the first half of the transition process in $0.35 \leq t/T \leq 0.37$, an increasing number of random turbulent spots occurs in the laminar base flow, leading to positive skewness. The start of transition can be detected by the deviation of the skewness from zero. For 50% intermittency, when the flow is exactly between the two flow states, the voltage signal changes equally between the laminar and the turbulent levels, resulting in a skewness

of zero ($x/c = 0.37$). For further progressing transition in $0.37 \leq t/T \leq 0.39$, the flow state is near turbulent with a reducing number of random laminar spots, resulting in negative skewness. The end of transition can be detected when the skewness is approaching zero again. For the relaminarization occurring in $0.65 \leq x/c \leq 0.69$, the skewness distribution develops vice versa with a positive peak following a negative peak.

It was possible to automate the detection of the beginning and the end of laminar and turbulent flow, and of 50% intermittency during transition and relaminarization. As long as the detection is applied to the skewness distribution derived from the voltage signal of a single pitching cycle, the method is based on the physical interpretation of the laminar/turbulent fluctuations in the boundary layer. If a phase-averaged voltage signal is used, the method does not allow a physical interpretation but provides very similar results compared to when the single-cycle detections are averaged afterwards. In this work, the detection was performed for the individual cycles, enabling the quantification of the scatter of the detected events. The results discussed in this work are the averaged values of 80 single cycle detections.

4 DETAILED TRANSITION ANALYSIS FOR THE PITCHING AIRFOIL

This section describes the detailed analysis of the unsteady transition characteristics of the pitching DSA-9A airfoil in subcritical flow. The transition movement can be well described using a test case with $\alpha = 4^\circ \pm 6^\circ$ and $k = 0.060$ ($f = 6.6\text{Hz}$) at $M = 0.3$ and $Re = 1.8 \times 10^6$. The Mach and Reynolds numbers represent flow conditions existing on the retreating blade during forward flight, and the pitching frequency is equal to the main rotor rotation frequency. The combination of mean angle of attack and amplitude is chosen so as to allow a transition movement completely over the hot film sheets both on the upper and on the lower model sides, enabling transition measurements with all hot film sensors.

4.1 Unsteady transition movement

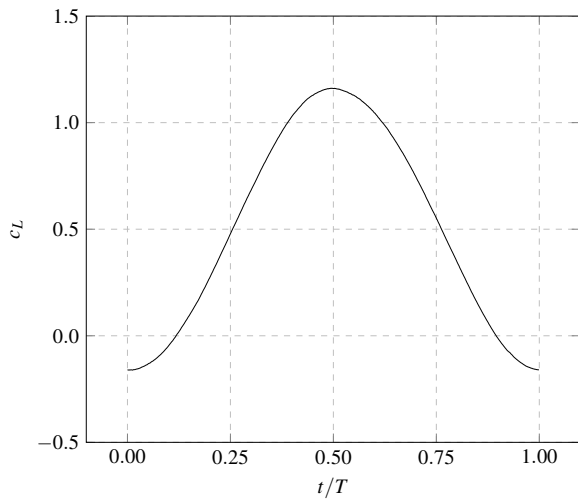
The unsteady transition movement on the upper and lower sides of the airfoil is presented in Fig. 5. Figures 5a and 5b show the distributions of the lift coefficient and indicate that the chosen test case has a sinusoidal lift curve and, therefore, no flow separation. The transition characteristics of the upper side are shown in Figs. 5c and 5d by the transition location plotted over the nondimensional time and the angle of attack, respectively. The characteristics of the lower side are given in Figs. 5e and 5f in the same manner. The symbols reflect the hot film sensor positions, and closed and open symbols represent the upstroke and the downstroke, respectively.

The transitions characteristics on the upper side, as shown in Figs. 5c and 5d, confirm the basic trends shown

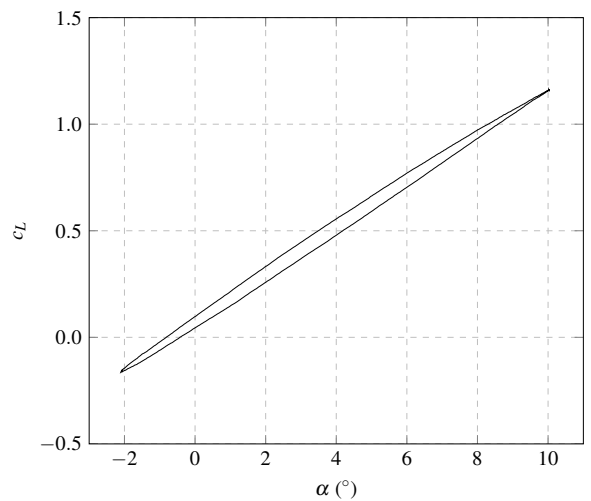
by other researchers [8, 6, 11]: the transition moves upstream with increasing angle of attack, and vice versa, developing a hysteresis between the upstroke and the downstroke, leading to enhanced laminar flow on the upstroke compared to the downstroke. A transitional zone can be identified on the upstroke and on the downstroke, since the onset of transition, 50% intermittency, and the end of transition are clearly separated events. A time delay can be seen between the transition movement and the model motion, with the transition movement following the model motion.

Transition moves on the upper side between $x/c = 0.01$ and the end of the hot film sheet. The leading edge sensor at $x/c = 0.00$ always showed laminar flow, whereas the sensor at $x/c = 0.01$ measured laminar, intermittent and, for a very short period, also turbulent flow. The most downstream clear indication of complete transition was found at $x/c = 0.65$, whereas no laminar flow was present at $x/c = 0.70$. This sensor signal was uncertain between intermittent and turbulent flow. The rate of the transition movement is rather mild as the transition needs nearly 40% of the cycle to change its position from $x/c = 0.65$ to $x/c = 0.01$, and vice versa. As an example, the location of 50% intermittency moves across this region in $\Delta t/T = 0.384$ ($\Delta\alpha = 11.24^\circ$) during the upstroke, and in $\Delta t/T = 0.350$ ($\Delta\alpha = -10.51^\circ$) on the way back during the downstroke. Significant parts of the DSA-9A upper side flow are in the intermittent flow state, similar to results shown by Richter et al. [11, 10] for the EDI-M109 airfoil at the same freestream conditions. The relations between the three transition parameters and the time or the angle of attack are also similar to results presented for EDI-M109 airfoil, however, with more transition movement existing on the DSA-9A airfoil, due to the different choice of test case.

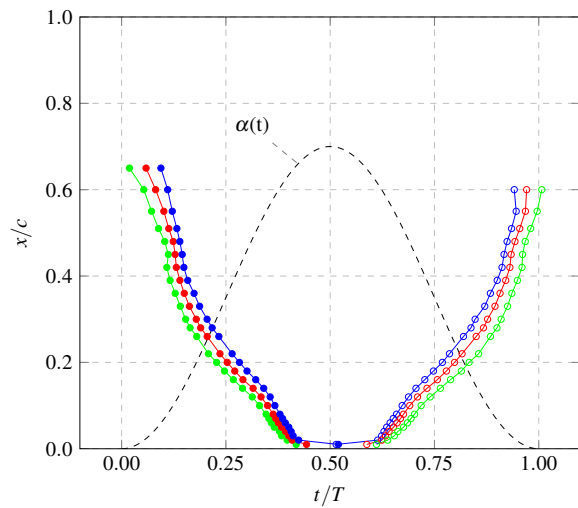
The transition on the lower side can also be represented by the three transition parameters, as shown in Figs. 5e and 5f. The transition movement is very different to that on the upper side. It has the opposite direction, as expected, and the rate of movement is significantly higher. The motion is dominated by a rapid jump between the leading edge and the trailing edge regions. The movement covers almost the entire lower surface as measured between $x/c = 0.03$ and the last operating sensor at $x/c = 0.945$. Upstream of $x/c = 0.03$, the sensor signals could not be analyzed. As for the upper side, a hysteresis develops between the upstroke and the downstroke, but on the lower side the hysteresis leads to reduced laminar flow on the upstroke compared to the downstroke. Again, a time delay between the transition movement and the model motion can be seen. The rapid changes in the transition location take place near the beginning and the end of the period, with 50% intermittency moving from $x/c = 0.05$ to $x/c = 0.86$ in only $\Delta t/T = 0.127$ ($\Delta\alpha = 3.55^\circ$) on the upstroke and back on the downstroke in $\Delta t/T = 0.081$ ($\Delta\alpha = -1.50^\circ$). During the rest of the cycle, the locations change only slightly, leading to laminar flow upstream of the tab on the lower side for the largest part of the period.



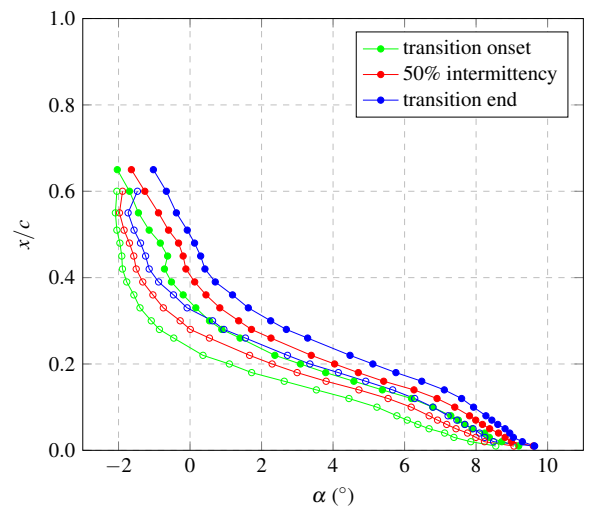
(a) Lift coefficient over time



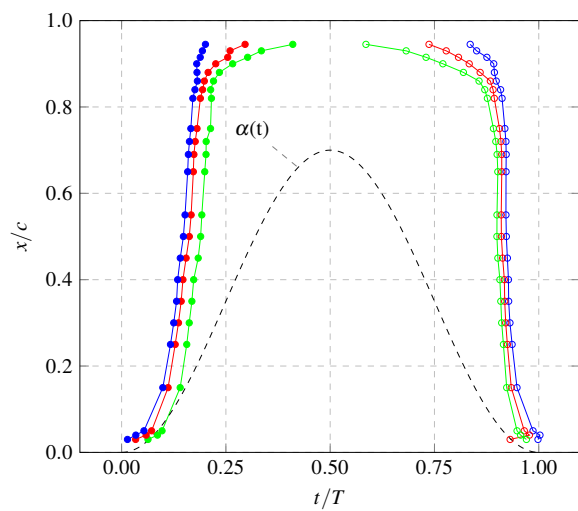
(b) Lift coefficient over angle of attack



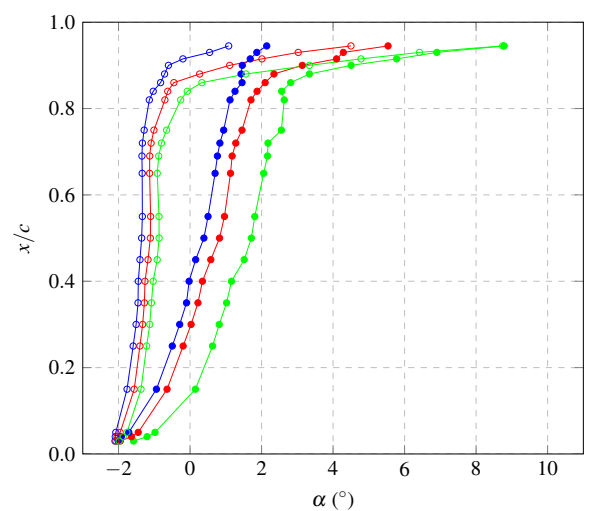
(c) Upper side: transition locations over time



(d) Upper side: transition locations over angle of attack

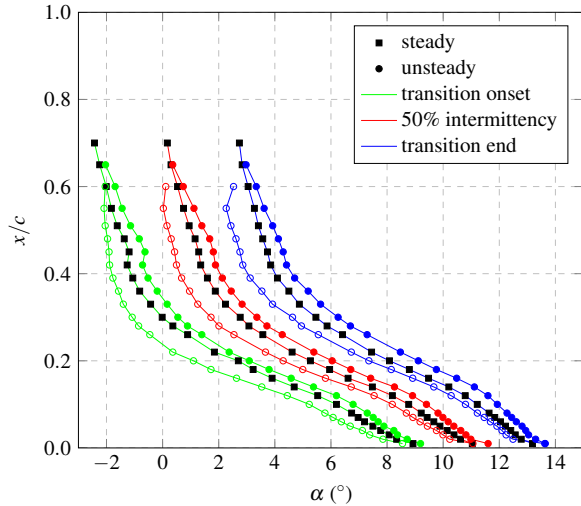


(e) Lower side: transition locations over time

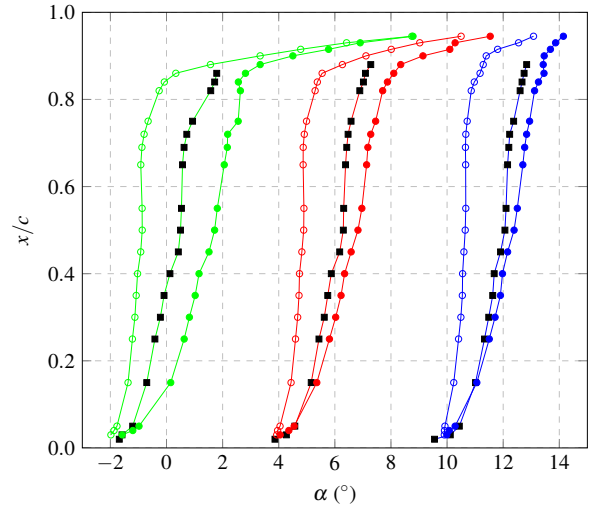


(f) Lower side: transition locations over angle of attack

Figure 5: Unsteady lift coefficient and transition parameters for $\alpha = 4^\circ \pm 6^\circ$, $k = 0.060$, $M = 0.30$, and $Re = 1.8 \times 10^6$ for upstroke (closed symbols) and downstroke (open symbols).



(a) Upper side: ($\alpha = \alpha_{onset}$, $\alpha = \alpha_{50} + 2^\circ$, $\alpha = \alpha_{end} + 4^\circ$)



(b) Lower side: ($\alpha = \alpha_{onset}$, $\alpha = \alpha_{50} + 6^\circ$, $\alpha = \alpha_{end} + 12^\circ$)

Figure 6: Comparison of steady and unsteady transition characteristics for $\alpha = 4^\circ \pm 6^\circ$, $k = 0.060$, $M = 0.30$, and $Re = 1.8 \times 10^6$

Figure 6 shows a comparison of the unsteady transition characteristics with the steady transition behavior. The steady behavior was measured in continuous but very slow angle of attack sweeps in order to allow the analysis of the hot film data in the same way as for the unsteady data. A pitch rate of $d\alpha/dt = 0.1^\circ/s$ was slow enough to ensure quasi-steady flow around the model. Figures 6a and 6b show the positions of transition onset, 50% intermittency and transition end plotted over the angle of attack. The curves of 50% intermittency and of the end of transition are shifted horizontally by $\Delta\alpha = 2^\circ$ and $\Delta\alpha = 4^\circ$ (Fig. 6a), respectively, for the upper side and by $\Delta\alpha = 6^\circ$ and $\Delta\alpha = 12^\circ$ (Fig. 6b), respectively, for the lower side to enhance the readability of the plots.

The steady transition is found to lie within the hysteresis loops of the unsteady transition both on the upper and on the lower side as expected. However, no consistent trend can be identified, which could have been helpful to transfer a steady transition behavior to a pitching airfoil. On the upper side, the steady onset of transition and steady 50% intermittency are both biased towards the upstroke. In contrast to this, the steady behavior of the end of transition comes close to the downstroke behavior at medium and high angles of attack. On the lower side, the trends are again different, with the steady behavior of transition onset approximately in the center of the unsteady hysteresis, but 50% intermittency and the end of transition are significantly nearer at the upstroke characteristics.

4.2 Length of the transition region

Most previous steady and unsteady transition investigations on airfoils, wings or rotor blades measured a single transition position. This gave a good estimation of the transition location but did not allow a more detailed analysis of the

transition region. It is known that the definition of a single transition point is not the correct physical interpretation of the transition phenomenon. Instead, the boundary layer progressively changes within a zone [14]. In the present work, the separate detection of the beginning and of the end of the transition process from a single hot film sensor signal, see Fig. 4, was performed for a large number of sensors. This allowed the determination of the size of the transition zone. For this purpose, the curves of transition onset and transition end shown in Figs. 5c to 5f were fitted with splines and the length of the transition region l was computed based on these splines. The results are shown in Fig. 7 with l/c plotted over the angle of attack for both sides and for the upstroke and the downstroke. In contrast to all previous plots, the symbols in Fig. 7 do not correspond to sensor positions, but only label the curves.

The results show that the transition zones on both sides of the pitching airfoil have substantial lengths even though the Reynolds number is high. Figure 7 indicates that the length of the transition zone on the lower side is significantly larger than on the upper side, and l/c is seen to change both with the angle of attack and with the motion of the model on both sides. Since the flow conditions $M = 0.3$ and $Re = 1.8 \times 10^6$ correspond to full scale conditions, it is expected that comparable sizes of the transition zone will also be reached when the DSA-9A airfoil is used on a rotor blade (as long as the influence of the rotation is small).

On the upper side, the length of the transition zone reduces with increasing angle of attack when the transition moves upstream towards the leading edge. The length changes from $l/c \approx 0.2$ at angles below zero to a very small size of $l/c \approx 0.01$ at $\alpha \approx 9^\circ$. The direction of motion has only small influence on l/c since the curves of upstroke and downstroke are similar. However, the size of the transition region is approximately 1% of chord larger during

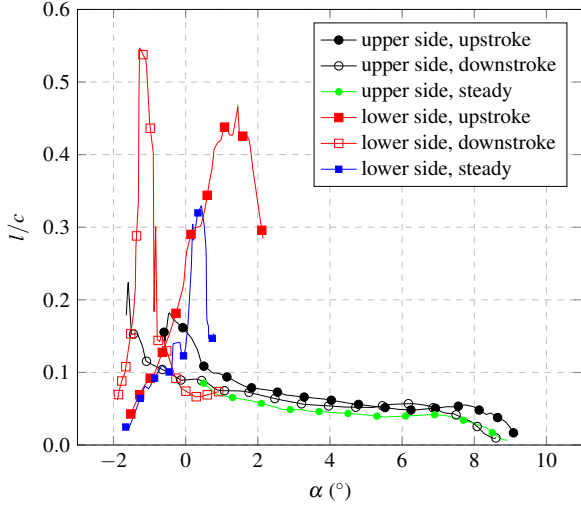


Figure 7: Length of the transition zone for $\alpha = 4^\circ \pm 6^\circ$, $k = 0.060$, $M = 0.30$, and $Re = 1.8 \times 10^6$

the upstroke than during the downstroke. Comparing the two curves closely, one can see that they are almost identical but have a shift in the angle of attack of approximately 1° . However, this α -shift cannot be found in the transition locations shown in Fig. 5d.

The behavior of the transition zone length on the lower side is dominated by the rapid jumps of the transition. These cause much larger transition zones and a higher influence of the direction of motion than on the upper side. While near the minimum angle of attack l/c is in the range of 4% chord (upstroke) to 7% chord (downstroke), the abrupt movements of the transition between the leading edge and the trailing edge regions cause strong increases in l/c , reaching maxima of $l/c \approx 0.43$ ($0.9^\circ \leq \alpha \leq 1.8^\circ$) during the upstroke and $l/c = 0.55$ ($\alpha = -1.2^\circ$) during the downstroke. On the upstroke, the transition movement is found to be initiated by a sudden downstream displacement of the end of the transition region, as can be seen in Fig. 5e. The beginning of the transition region follows with a small time delay, resulting in an extreme spreading of the transition zone. When the end of the zone reaches the region on the airfoil upstream of the tab, its further downstream motion is slowed down. Since the beginning of the transition zone follows rapidly, the transition zone shortens again. During the downstroke, the progression of the upstream transition zone movement happens opposite compared to the upstroke. First the beginning of the transition region starts its rapid movement from the trailing edge to the leading edge, followed by the end of the transition zone. Since the gradients of the movement $d(x/c)/dt$ and $d\alpha/dt$ are higher during the downstroke than during the upstroke for this test case, see Fig. 5e, the transitional zone is spread even more and a higher l/c -maximum is reached. After the beginning of the transition zone reached the leading edge region, l/c reduces significantly.

The size of the transition zone at steady flow conditions

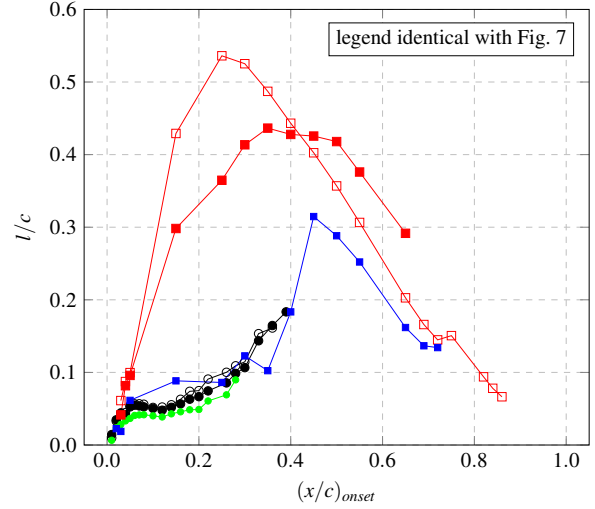


Figure 8: Length of the transition zone for $\alpha = 4^\circ \pm 6^\circ$, $k = 0.060$, $M = 0.30$, and $Re = 1.8 \times 10^6$

is found to be similar to the unsteady behavior. Figure 7 also shows the steady l/c for both airfoil sides, indicating that the size of the steady transition zone on the upper side corresponds well to the unsteady behavior during the downstroke. In contrast to this, the steady size on the lower side better matches the unsteady behavior during the upstroke. However, a significantly lower $(l/c)_{max}$ is reached for the steady case since the characteristics of the abrupt transition movement on the lower side is slightly different between the steady and the unsteady case.

Figure 8 shows l/c plotted over the onset position of the transition zone $(x/c)_{onset}$ in order to discuss the size of the transition region depending on where it starts on the airfoil surface. The style of the curves is identical with the one in Fig. 7, with the exception that the symbols represent sensors locations again. The results show that when the transition occurs near the leading edge, a small but noticeable transition zone develops both on the upper and on the lower side. Starting from a length of approximately 1% chord for a transition onset at $x/c = 0.01$, l/c increases with increasing distance from the leading edge on both sides. The rates of increase are significantly different between the upper and the lower sides, and they are influenced by the direction of the pitching motion on the lower side in addition.

On the upper side, the size of the transition zone increases to approximately 18% chord for an onset at $x/c = 0.39$. The differences between the upstroke and the downstroke observed in Fig. 7 almost vanish in Fig. 8. This means that the transition zone maintains the same characteristics, regardless whether the transition moves upstream or downstream during the downstroke or the upstroke, respectively. Transition zones starting further downstream of $(x/c)_{onset} = 0.39$ could not be evaluated since the end of the zones were outside of the hot film sensor array. The detailed development of the transition zone in the leading

edge region shows a particularly interesting result: a delay in the growth of the transition region occurs in $0.06 \leq x/c \leq 0.12$, where l/c actually even reduces by 1% chord. This behavior is confirmed by the measurements both on the upstroke and on the downstroke. However, no reason for this delay could be found.

On the lower side, the rate of the l/c -increase downstream of the leading edge is found to be much larger than on the upper side. A strong dependency also occurs on direction of motion as the increase is stronger during the downstroke than during the upstroke. On the upstroke, a maximum size of the transition zone on the order of 41% to 44% chord is measured for $0.30 \leq (x/c)_{onset} \leq 0.50$, before l/c reduces further downstream. Combining this information with the previous findings about the development of the transition movement, it can be concluded that the abrupt shift of the transition from the leading to the trailing edge starts with a downstream spreading of the transition zone until a physical limit of the length of the region is reached at $(x/c)_{onset} \approx 0.30$. This is followed by a shift of the transition zone maintaining an approximately constant size until $(x/c)_{onset} \approx 0.50$. At this moment, the end of the transition zone reaches the trailing edge region, and the zone is shrinking with the beginning of the zone moving towards the end.

Unlike on the upper side, the transition zone on the lower side has a different behavior during its upstream movement (downstroke) than during its downstream movement (upstroke). During the downstroke, the maximum of l/c increases even further to $\sim 53\%$ chord reached with a transition onset position of $x/c = 0.25$. However, no constant transition zone size was measured. Instead, the transition zone is smaller for $(x/c)_{onset} > 0.4$ during the downstroke than during the upstroke and it is larger further upstream.

Comparing the size of the transition region for steady and unsteady conditions in Fig. 8, a very similar behavior occurs on the upper side but the size of the steady transition region is always slightly smaller than in the unsteady case. This means that the unsteady airfoil motion leads to a growth of the transition region compared to steady flow, both during the upstroke and the downstroke. On the lower side, very large differences between the steady and unsteady results occur and a qualitative similarity is hard to see. The steady l/c is always smaller than either one of upstroke and downstroke, too, and it is significantly smaller for transition onset upstream of 40% chord. Downstream, the steady behavior approaches the one of the downstroke.

The absence of the influence of the upstroke/downstroke motion on the upper side transition zone characteristics deserves some additional attention. Figure 9 shows the upper side pressure distributions for the angles of attack that correspond to the transition onset positions of $x/c = 0.12$ and $x/c = 0.39$ on the upper side. The pressure distributions with a transition onset at $x/c = 0.39$ show a stagnation point since the angle of attack is negative. The closed and open symbols represent the upstroke and the downstroke, respectively. It can be seen that, although there is no dif-

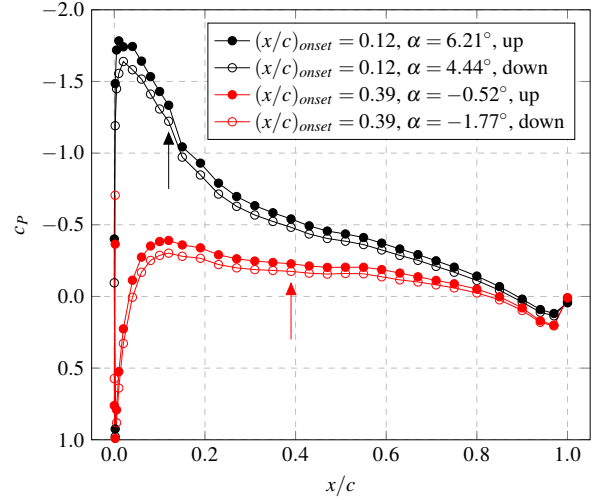


Figure 9: Upper side pressure distributions for select transition onset positions for $\alpha = 4^\circ \pm 6^\circ$, $k = 0.060$, $M = 0.30$, and $Re = 1.8 \times 10^6$

ference in the transition region, the pressure distributions of upstroke and downstroke are not identical. The upstroke pressure distribution always has a much higher angle of attack and, correspondingly, the distributions show changes in the strength of the suction peak. Despite these changes, the position and the size of the transition region is constant as it can partly also be identified by the kinks in the pressure distributions. The transition onset positions measured by the hot film sensors are marked with arrows. Comparing the pressure gradients $dc_p/d(x/c)$ upstream of the transition onset positions, it was found that the gradient is different for the selected angles of attack, too. It is therefore assumed that the distributions shown have different boundary layer profiles which counteract the different pressure gradients, resulting in the same transition behavior.

4.3 Intermittent flow

The flow inside of the transition region is neither fully laminar nor fully turbulent, thus, the boundary layer state of the intermittent flow is undefined. The amount of intermittent flow existing on the pitching airfoil is of special interest since state-of-the-art numerical transition prediction tools do not physically model this intermittent flow region. Instead, the boundary layer change is mostly defined by a single transition point and a numerical transformation of the boundary layer follows based on the turbulence production of the CFD method. This kind of boundary layer change is not related to the real physical development.

The discussion of the length of the transition zone already showed that significant intermittent flow zones exist on both sides of the pitching DSA-9A airfoil. The hot film data measured in this work can furthermore be used to analyze the time span in which a sensor is exposed to intermittent flow as well as the change in angle of attack the airfoil experiences during this time span. The results are shown in

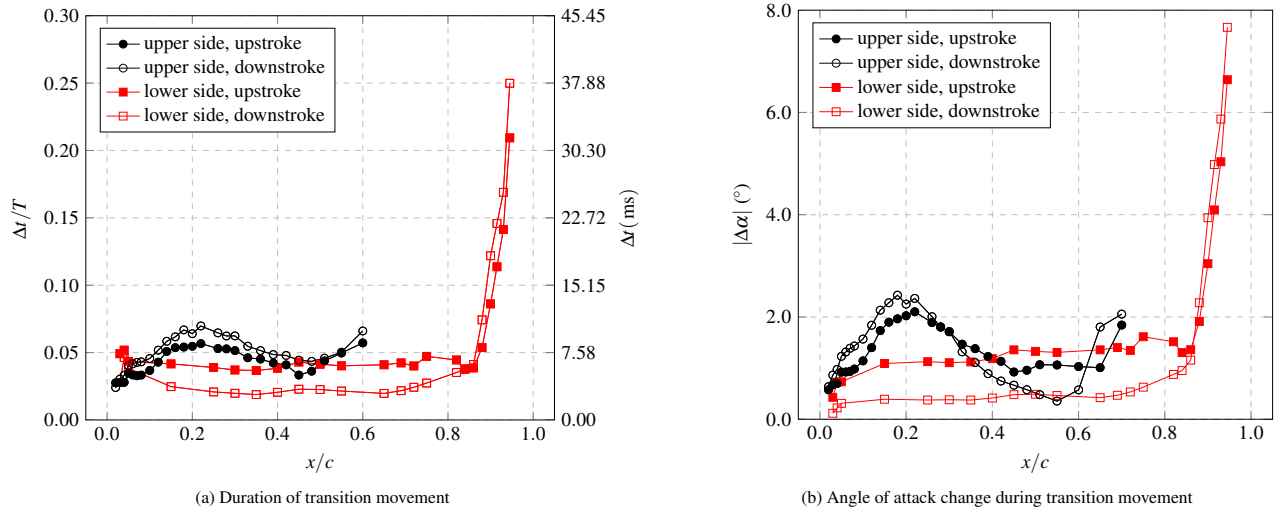


Figure 10: Time span and angle of attack change during transition movement for $\alpha = 4^\circ \pm 6^\circ$, $k = 0.060$, $M = 0.30$, and $Re = 1.8 \times 10^6$

Figure 10 with the portion of the period $\Delta t/T$ of intermittent flow plotted over the sensor location x/c in Fig. 10a. The real time span Δt is plotted on the second vertical axis in addition. The results show that intermittent flow exists for significant portions of the period and that $\Delta t/T$ depends on the direction of the transition movement relative to the flow direction as $\Delta t/T$ reduces when the transition movement and the flow are in opposite directions.

On the upper side in Fig. 10a, the qualitative behavior of $\Delta t/T$ is independent of the direction of the pitching motion. However, intermittent flow exists for a longer time span on the downstroke at a given coordinate compared to the upstroke. A roughly constant offset of $\Delta t/T = 0.007$ ($\Delta t \approx 1$ ms) occurs, indicating that the transition needs more time to pass during pitch down, when it moves with the flow direction, than during pitch up, when it moves in the opposite direction. The movement of the transition is generally faster against the main flow direction, which corresponds to the gradients of the transition curves shown in Fig. 5.

No uniform trend between $\Delta t/T$ and x/c can be seen in Fig. 10a on the upper side. Starting from the shortest time span $\Delta t/T \approx 0.025$ at the leading edge for both upstroke and downstroke, maxima are reached at $x/c = 0.22$ with $\Delta t/T = 0.057$ and $\Delta t/T = 0.070$, respectively. At this position, intermittent flow exists for 5.7% of the period during the upstroke and 7.0% during the downstroke, leading to 12.7% during the entire period. In contrast to this, a clear reduction of $\Delta t/T$ happens downstream between $x/c = 0.22$ and $x/c = 0.46$ although the size of the transition zone increases in this part of the airfoil. Local minima of $\Delta t/T$ are reached at $x/c = 0.46$ with values similar to the ones existing for the very small transition zones near the leading edge. The speed of the transition movement enhances approximately by a factor of 3 in this region. Downstream of $x/c = 0.46$, $\Delta t/T$ increases again.

The data ends at $x/c = 0.60$ since this sensor was the most downstream sensor at which the full development of transition and relaminarization could be measured.

On the lower side in Fig. 10a, the behavior is essentially different since x/c only has a minor influence on $\Delta t/T$ for the largest part of the airfoil and strong changes occur in the trailing edge region. Upstream of $x/c = 0.86$, the time spans are a little smaller than on the upper side. Almost constant periods of intermittent flow of approximately 4% and 2% of the period exist during the upstroke and the downstroke, respectively. Thus, an almost constant offset between pitch up and pitch down exists also on the lower side, but with $\Delta t/T \approx 0.018$ ($\Delta t \approx 2.7$ ms) it is almost three times as large as on the upper side. Since the transition movement on the lower side happens in the opposite direction compared to the upper side, the transition movement against the main flow direction (downstroke) is again faster than in the same direction (upstroke). In the trailing edge region, an exponential increase in $\Delta t/T$ occurs for the upstroke and downstroke in the same manner. The transition movement slows down seriously, leading to significantly higher periods of intermittent flow of up to $\Delta t/T = 0.25$ ($\Delta t \approx 37.9$ ms) at the last sensor at $x/c = 0.935$. Therefore, the rear part of the lower side happens to be in intermittent flow between 25% and 50% of the entire oscillation period.

In Fig. 10b the duration of intermittent flow is converted into the angle of attack change $\Delta\alpha$ that occurs during the intermittent flow zone passes a sensor. The graph is certainly similar to Fig. 10a but provides valuable information about the unsteadiness of the flow at a specific position on the airfoil compared to steady conditions. While of course no change in α occurs during transition on static airfoils, $|\Delta\alpha|$ is significant on a pitching airfoil. On the upper side, $|\Delta\alpha|$ varies between $|\Delta\alpha| \approx 0.4^\circ$ and $|\Delta\alpha| \approx 2.4^\circ$. On the lower side, chordwise differences are again less pronounced upstream of the trailing edge region, where slightly increas-

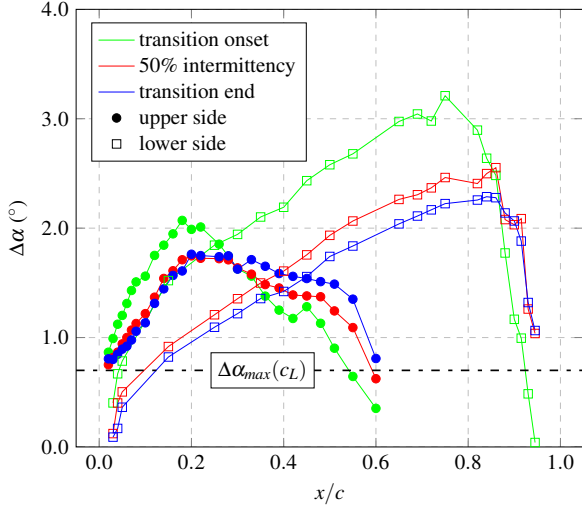


Figure 11: Hysteresis between upstroke and downstroke for $\alpha = 4^\circ \pm 6^\circ$, $k = 0.060$, $M = 0.30$, and $Re = 1.8 \times 10^6$

ing values of up to $|\Delta\alpha| \approx 1.5^\circ$ occur. In the trailing edge region, however, the α -change that occurs during intermittent flow exists in this region increases to an extraordinary $|\Delta\alpha| \approx 7.7^\circ$ for both the upstroke and the downstroke.

4.4 Hysteresis

The degree of unsteadiness of the transition becomes visible when the hysteresis between the upstroke and the downstroke is analyzed, and when it is compared with the unsteadiness of the lift coefficient. Figure 11 shows the differences in the angles of attack at which transition occur between the upstroke and the downstroke ($\Delta\alpha = \alpha_{upstroke} - \alpha_{downstroke}$) plotted over the sensor position. In addition, the maximum α -change of the lift coefficient $\Delta\alpha_{max}(c_L) = 0.7^\circ$ is also plotted. The results show that for the pitching frequency $f = 6.6\text{Hz}$ ($k = 0.060$), which represents a main rotor frequency of small helicopters very well, the transition hysteresis is significant for both airfoil sides and strongly depends on the chordwise position on the airfoil. It is much larger than the maximum change caused by the unsteadiness in lift, indicating that the unsteady transition behavior is not just caused by the lift hysteresis. Keeping in mind that the performance prediction of state-of-the-art helicopter aeromechanics codes [15] is usually based on steady airfoil performance data (including steady transition characteristics) with a correction for pitching airfoils mostly after Theodorsen [16], no larger hysteresis than the one of c_L can be expected in the results of these codes. Thus, changes in the airfoil performance due to significant unsteady transition characteristics are currently not included.

Figure 11 shows that the hysteresis is larger on the lower side than on the upper side. On the upper side, 50% intermittency and the end of transition show a very similar behavior, with a strongly increasing $\Delta\alpha$ between the leading edge and $x/c = 0.20$, reaching a maximum of $\Delta\alpha \approx 1.8^\circ$.

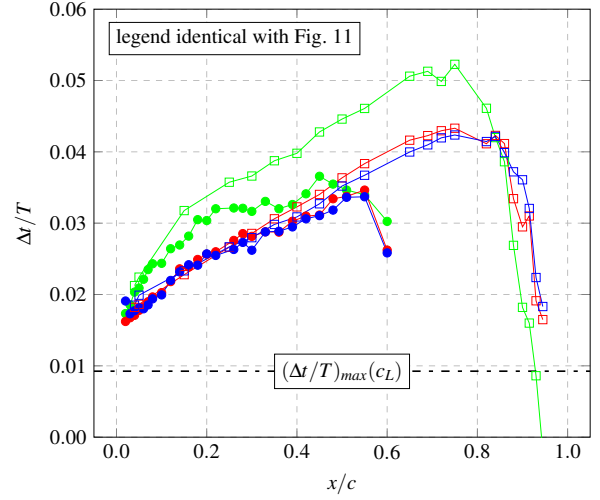


Figure 12: Time delay between the transition and the model motion for $\alpha = 4^\circ \pm 6^\circ$, $k = 0.060$, $M = 0.30$, and $Re = 1.8 \times 10^6$

This means that the end of transition occurs at 1.8° higher angle of attack on the upstroke than on the downstroke at this position. Further downstream, $\Delta\alpha$ reduces and reaches values near $\Delta\alpha = 0.7^\circ$ at the end of the analyzed region. On the lower side, a linear increase of $\Delta\alpha$ occurs over the largest part of the airfoil, followed by a sharp drop of $\Delta\alpha$ in the trailing edge region. 50% intermittency and the end of transition again show a very similar behavior. The hysteresis of the onset of transition has a higher sensitivity on both sides of the airfoil. It reaches higher values of $\Delta\alpha$ than the other parameters, with $\Delta\alpha_{max} = 2.1^\circ$ on the upper side and $\Delta\alpha_{max} = 3.2^\circ$ on the lower side.

4.5 Time delay

Previous investigations of Richter et al. [10, 11] on the upper side of the EDI-M109 airfoil indicated that a time delay occurs between the temporal transition movement and the motion of the model. The delay $\Delta t/T$ seemed to be constant for several test cases with constant pitching frequency but different combinations of mean angles of attack and amplitudes. The movement of the transition was found to be approximately symmetric for the upstroke and the downstroke when plotted over the time, and the time delay was calculated from the data measured at the most downstream transition position. For the same pitching frequency as in this work, the delay was determined to $\Delta t/T = 0.024$.

The data measured in this work allowed a more detailed investigation of the time delay. The delay was calculated for the three transition parameters at each sensor position:

$$\Delta t/T = \frac{(t/T)_{upstroke} + (t/T)_{downstroke}}{2} - \frac{1}{2} \quad (2)$$

The results are plotted in Fig. 12 with the same style of the curves as in Fig. 11. The results show that no constant time delay exists over the airfoil chord. Therefore, the up-

stroke/downstroke transition movement is not symmetric, although especially Fig. 5c leaves this impression at the first glance. The time delay has a significant linear increase over the largest part of the airfoil both for the upper and for the lower side, and the sensitivity of the onset of transition of x/c is again larger than those of the other two transition parameters.

At the leading edge, a small time delay of approximately $\Delta t/T = 0.017$ occurs equally on both sides of the airfoil and for both the upstroke and the downstroke. The time delays calculated for 50% intermittency and for the end of transition increase almost identical to maximum values of $\Delta t/T \approx 0.035$ at $x/c = 0.55$ on the upper side and $\Delta t/T \approx 0.043$ at $x/c = 0.75$ on the lower side. The onset of transition again reaches higher maximum values, instead, with $\Delta t/T \approx 0.037$ on the upper side and $\Delta t/T \approx 0.052$ on the lower side. Evaluating $\Delta t/T$ at the most downstream transition location on the upper side as it was done in [10, 11], a time delay of $\Delta t/T \approx 0.026$ occurs for this test case. This is very similar to the delay measured for the EDI-M109 airfoil.

The time delay was also computed for the unsteady lift coefficient and the maximum $(\Delta t/T)_{max}(c_L) = 0.009$ is additionally shown in Fig. 12. Similar to the hysteresis in Fig. 11, the time delay due to the unsteadiness of the transition is much larger than the maximum time delay caused by the unsteadiness in lift.

4.6 Unsteadiness

On a pitching airfoil, the transition location constantly moves over the airfoil for the largest part of the pitching cycle. This means that the transition zone moves even while a fluid element goes through it. The degree of unsteadiness of the transition mechanism can be examined if the movement of the transition zone is related to the motion of a fluid element during it travels through the transition zone with freestream velocity. Figure 13 shows the displacement $\Delta x/c$ of the transition region on the airfoil during the passage of this fluid element plotted over the onset position of the transition $(x/c)_{onset}$. In this approach, the varying sizes of the transition zone as well as the varying speeds of the transition movement over the airfoil are respected. The use of the freestream velocity is a simplification that is done since the consideration of the local flow speed is too complicated.

The results in Fig. 13 show that the movement of the transition zone on the upper side is quasi steady compared to the motion of the fluid element and there is no difference between the upstroke and the downstroke. The displacement is very close to zero ($\sim 0.1\%$ chord) near the leading edge and increases slightly with an increasing $(x/c)_{onset}$ to a maximum of $\Delta x/c \approx 0.007$ at $(x/c)_{onset} = 0.39$. This means that the transition zone starting at this position on the upper side moves only 0.7% chord while the fluid element goes through it. Thus, a quasi-steady transition behavior can be assumed on the upper side, which allows the

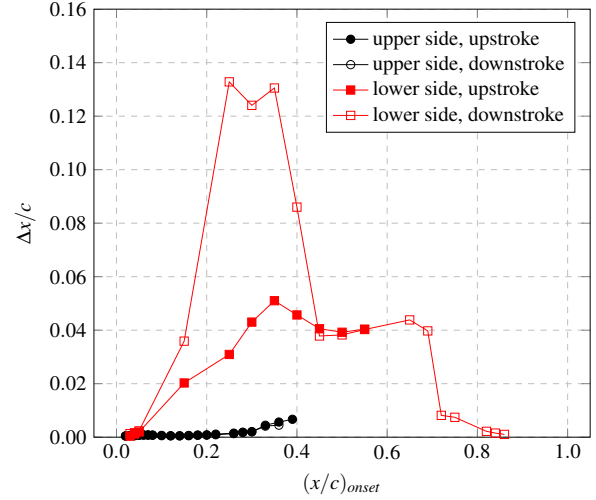


Figure 13: Displacement of the transition zone during passage of a fluid element for $\alpha = 4^\circ \pm 6^\circ$, $k = 0.060$, $M = 0.30$, and $Re = 1.8 \times 10^6$

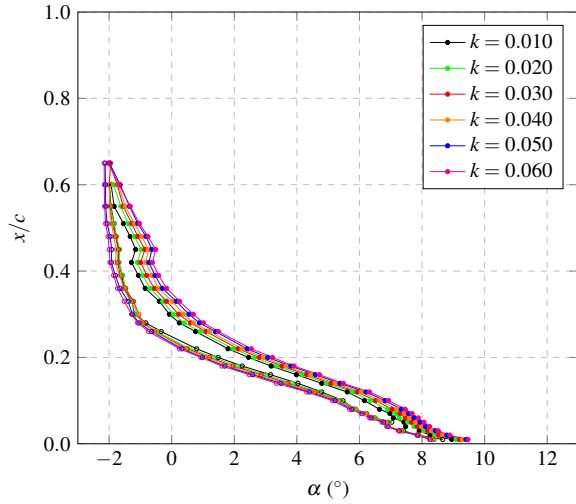
use of quasi-steady transition prediction tools in a numerical simulation. On the lower side, much more unsteadiness is revealed. Since the transition movement happens much faster, much higher values of $\Delta x/c$ occur and differences between the upstroke and the downstroke become visible in addition. During the passage of the fluid element, the transition zone moves by a maximum of as much as 13% of chord on the downstroke. On the upstroke, significantly lower values are reached but still a maximum of 5.2% chord occurs. Thus, the transition behavior on the lower side is seen to be really unsteady, and we can expect that quasi-steady transition prediction will encounter problems here.

5 INFLUENCE OF THE PITCHING FREQUENCY

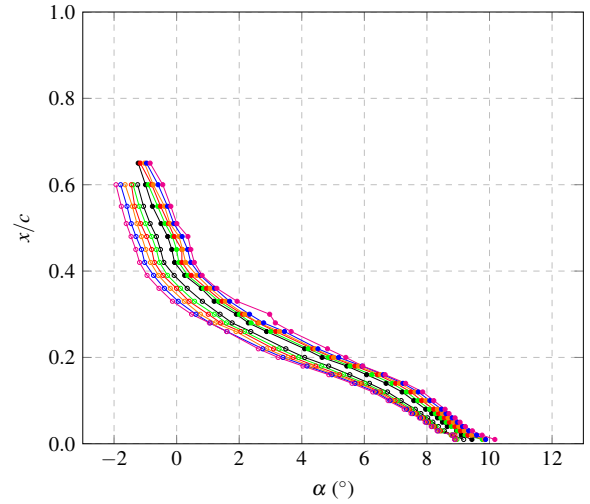
The influence of the pitching frequency on the unsteady transition was investigated for a model motion of $\alpha = 5^\circ \pm 7^\circ$ at $M = 0.3$ and $Re = 1.8 \times 10^6$. The frequency was varied in $0.010 \leq k \leq 0.060$ ($1.1 \text{ Hz} \leq f \leq 6.6 \text{ Hz}$) with steps of $\Delta k = 0.010$ ($\Delta f = 1.1 \text{ Hz}$). The frequency effect will be discussed with respect to changes in the unsteady transition movement, the size of the transition region, the intermittent flow, and the time delay between the transition movement and the model motion.

5.1 Unsteady transition movement

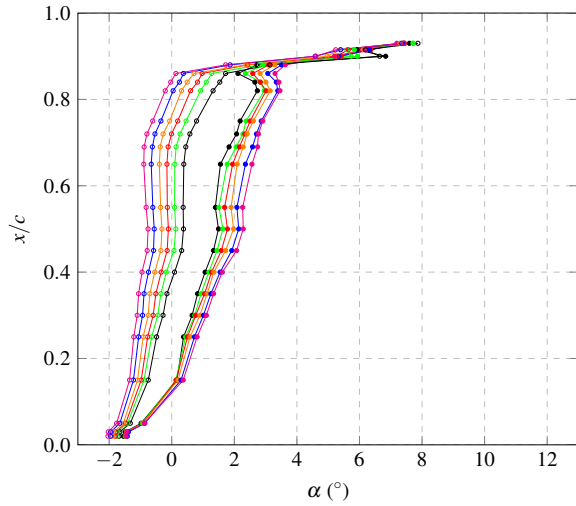
The influence of the pitching frequency is shown in Fig. 14 by the locations of the onset and the end of the transition zone plotted over the angle of attack for both sides of the airfoil, and for the six reduced frequencies investigated. The steady transition behavior is shown in addition. The results indicate that the frequency has a large effect on the transition characteristics in general, leading to an increase in the hysteresis between the upstroke and the downstroke



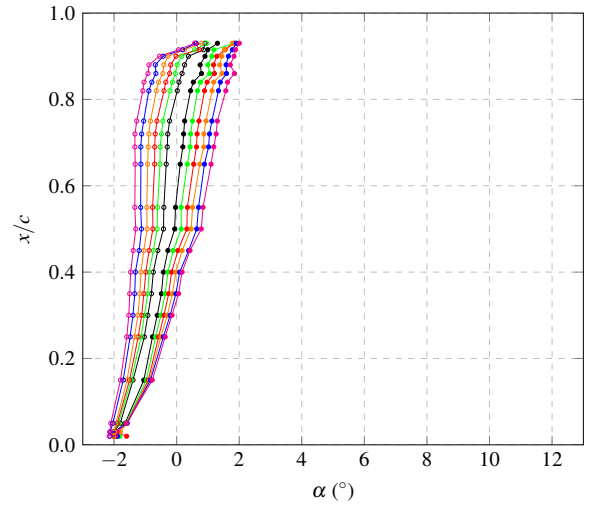
(a) Location of transition onset on the upper side



(b) Location of transition end on the upper side



(c) Location of transition onset on the lower side



(d) Location of transition end on the lower side

Figure 14: Transition parameters for a frequency sweep with $\alpha = 5^\circ \pm 7^\circ$, $M = 0.30$ and $Re = 1.8 \times 10^6$ for upstroke (closed symbols) and downstroke (open symbols).

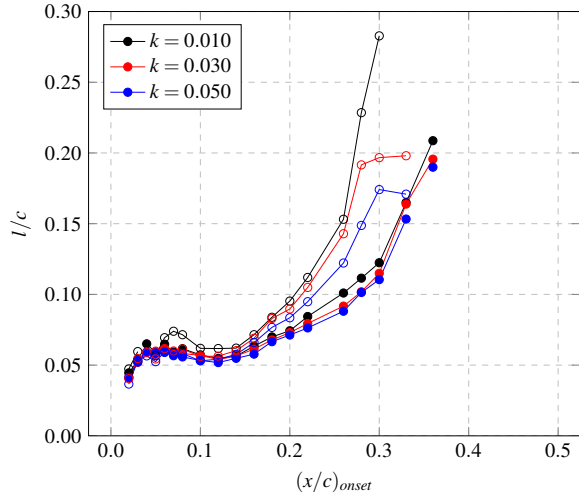
on both sides of the airfoil. These findings confirm and expand the findings of previous studies [6, 8] in which the frequency effect on a single transition point was discussed for the upper side of pitching airfoils.

On the upper side of the DSA-9A airfoil, the frequency effect is different for the onset and the end of transition, and it depends on the direction of the movement in addition. The transition onset shows a very similar behavior for all frequencies during the upstroke, shown in Fig. 14a. An increasing $\Delta\alpha$ is caused by the increasing frequency, leading to a delay of the transition onset to higher angles of attack. The α -offset is slightly larger in the front part of the airfoil than in the central part. For the highest frequency $k = 0.060$, $\Delta\alpha \approx 0.7^\circ - 0.8^\circ$ exists compared to the lowest frequency $k = 0.010$. Analogously, the frequency effect results in a reduction of the onset angle of attack on the downstroke, i.e. transition happens earlier. With

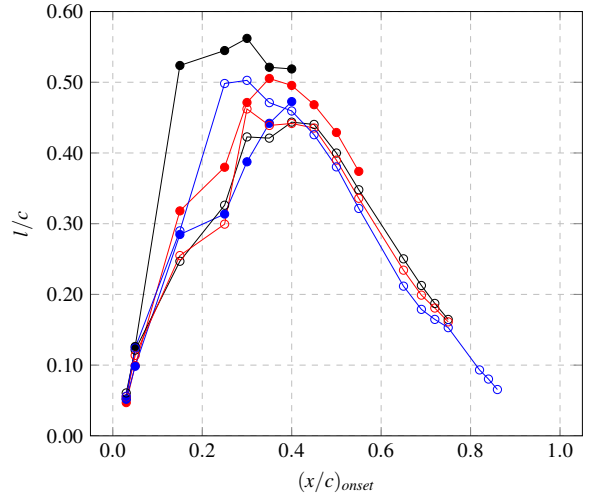
a maximum of only $\Delta\alpha \approx -0.3^\circ$ between $k = 0.010$ and $k = 0.060$, this effect is smaller than the frequency effect during the upstroke and it vanishes near the leading edge.

The end of transition, shown in Fig. 14b, exhibits a frequency effect similar to the one of the onset of transition. On the upstroke, an α -offset occurs nearly independent of x/c , delaying the end of transition to higher angles of attack, with $\Delta\alpha \approx 0.7^\circ$ for $k = 0.060$. On the downstroke, the influence on the end of transition is larger than the effect on the onset. $\Delta\alpha \approx -0.9^\circ$ is reached for $k = 0.060$ in the central part of the upper side, and the influence does not vanish near the leading edge. Instead, a small offset of $\Delta\alpha \approx -0.2^\circ$ remains for the highest frequency investigated.

On the lower side, the influence of the frequency is again similar, shifting the onset and the end of transition to higher α on the upstroke and to lower α on the downstroke. How-



(a) Size of the transition zone on the upper side



(b) Size of the transition zone on the lower side

Figure 15: Frequency effect on the size of the transition zone for $\alpha = 5^\circ \pm 7^\circ$, $M = 0.30$, and $Re = 1.8 \times 10^6$ for upstroke (closed symbols) and downstroke (open symbols)

ever, the effect is generally larger than on the upper side and shows a clear dependency of x/c as $\Delta\alpha$ increases significantly from the leading edge to the trailing edge. The onset of transition has no frequency effect near the leading edge during the upstroke, as shown in Fig. 14c, and $\Delta\alpha$ increases almost linearly with x/c . In the trailing edge region at $x/c = 0.86$, a maximum of $\Delta\alpha \approx 1.1^\circ$ is reached between $k = 0.010$ and $k = 0.060$, whereas $\Delta\alpha$ reduces further downstream. On the downstroke, a small frequency effect on the onset of transition of $\Delta\alpha \approx -0.4^\circ$ persists near the leading edge. $\Delta\alpha$ again increases with increasing x/c and reaches $\Delta\alpha \approx -1.6^\circ$ at $x/c = 0.86$. For the end of transition, shown in Fig. 14d, the influence of the frequency on the upstroke and on the downstroke is very similar, starting from a small $\Delta\alpha$ at the leading edge and reaching approximately $\Delta\alpha = -1^\circ$ between the highest and the lowest frequency at $x/c = 0.86$.

5.2 Length of the transition zone

The main influence of the pitching frequency on the length of the transition zone is seen in a shortening of the zone with increasing frequency. This happens on the upper side, and on the lower side during the upstroke, and the effect on the lower side is larger than on the upper side. Figure 15 shows the transition zone size l/c plotted over the onset position of the transition $(x/c)_{onset}$. For better readability, only three reduced frequencies $k \in [0.010, 0.030, 0.050]$ are shown.

On the upper side, shown in Fig. 15a, hardly any influence of the frequency can be seen in the front part of the airfoil in $(x/c)_{onset} \leq 0.16$. Further downstream, a nearly constant small reduction in the length of $\Delta l/c = 0.01$ occurs between the $k = 0.010$ and $k = 0.050$ during the upstroke. During the downstroke, a larger frequency effect

occurs. The length of the transition zone reduces both with frequency and with the onset position, leading to a significant reduction in the maximum sizes from $l/c = 0.28$ to $l/c = 0.17$.

On the lower side, shown in Fig. 15b, the influence of the frequency is more complex. While the influence vanishes near the leading and the trailing edges, both the maximum length of the zone and the onset position at which this zone starts clearly change with k . With increasing frequency during the downstroke, the maximum size reduces and the onset position of $(l/c)_{max}$ is shifted downstream. For the lowest frequency, the transition zone has a maximum length of $\sim 53\%$ chord with an onset position in the range of $0.15 \leq (x/c)_{onset} \leq 0.40$. Increasing to $k = 0.050$ leads to a reduction of $(l/c)_{max}$ to $\sim 44\%$ chord, and the maximum only occurs at $(x/c)_{onset} = 0.40$. On the downstroke, the maximum length increases from 44% to 50% chord with increasing k , and the onset position moves upstream. The frequency effect reduces further downstream of $(x/c)_{onset} = 0.4$, and a small but almost constant reduction of l/c occurs with increasing frequency.

For slowed rotor concepts of new helicopters, which use a reduced rotation rate in order to exploit benefits with respect to the rotor aeroacoustics, the results of this work indicate that the amount of transitional flow can increase on both the upper and the lower sides of the blades due to the reduced rotation frequency.

5.3 Intermittent flow

Due to changes in the transition zone length and in the rate of the transition movement with varying pitching frequency, the part of the period in which intermittent flow occurs at a selected position is also affected. The main effect can be seen in a consistent reduction of $\Delta t/T$ on both

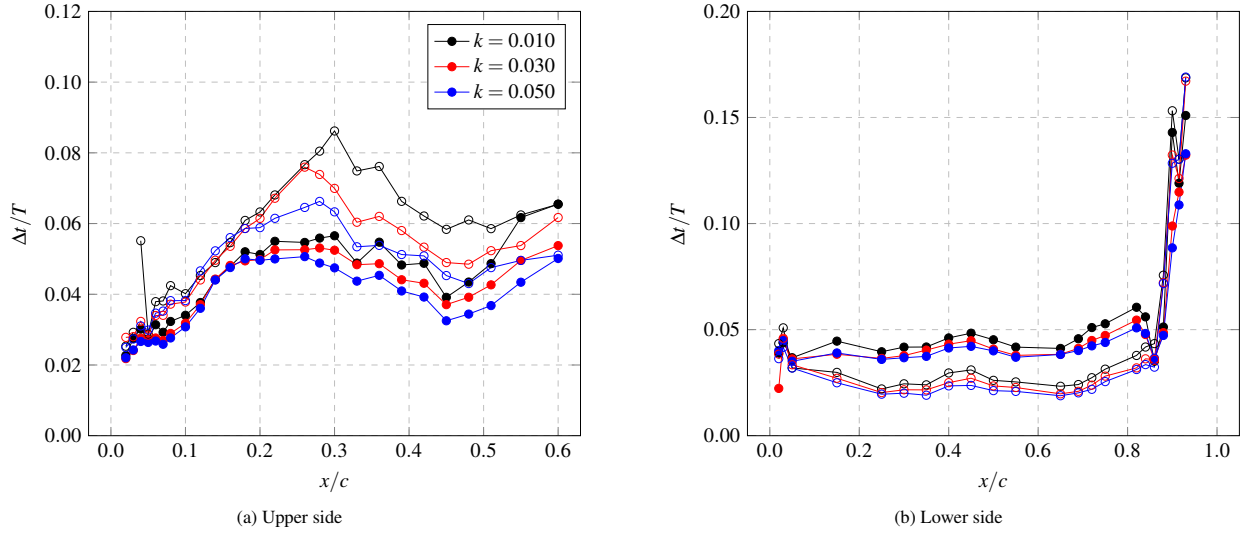


Figure 16: Frequency effect on the time span of intermittent flow for $\alpha = 5^\circ \pm 7^\circ$, $M = 0.30$, and $Re = 1.8 \times 10^6$ for upstroke (closed symbols) and downstroke (open symbols)

airfoil sides and for both the upstroke and the downstroke, although the unsteadiness of the flow increases with increasing frequency. This is caused by a reduction of the size of the transition zone primarily on the upper side, on the one hand. On the other hand, the additional increase in the speed of the transition movement, especially on the lower side, leads to a reduction of $\Delta t/T$ even though the transition zone increases in some conditions.

Figure 16 shows the behavior of $\Delta t/T$ over x/c for the same selected reduced frequencies as discussed before. Similar to the length of the transition zone in Fig. 15, the $\Delta t/T$ shows hardly any frequency effect upstream of $x/c = 0.18$ on the upper side, whereas significant changes occur downstream. The effect is largest during the downstroke on the upper side with a reduction of the $(\Delta t/T)_{max}$ by approximately 25% when the frequency is increased from $k = 0.010$ to $k = 0.050$. The effects on the upper side during the upstroke and on the lower side in general are found to be in the same order of magnitude. In the trailing edge region on the lower side, the influence of the frequency vanishes again.

5.4 Time delay

The influence of the frequency on the time delay between the transition movement and the model motion is shown in Fig. 17 based on the results obtained for 50% intermittency. All six investigated frequencies are shown. Similar to the findings presented in section 4.5, the curves extracted for the different test cases show an approximately linear behavior for both sides of the airfoil and regardless of the pitching frequency. The frequency effect is found to consist of both an increasing shift $\Delta t/T$ to higher time delays with increasing k , and of an increasing slope of the curves. This leads to an exaggerated increase of the time delay both with increasing frequency and with increasing

coordinate on the airfoil. As an example, for $k = 0.010$ an increase in the time delay by 0.3% of the period occurs between $x/c = 0.02$ and $x/c = 0.51$ on the upper side, whereas it is 1.9% for $k = 0.060$. The same behavior exists on the lower side, where an increase of 0.4% of the period occurs between $x/c = 0.03$ and $x/c = 0.82$ for $k = 0.010$, whereas it is 3.6% for $k = 0.060$.

The assumption that a constant time delay between the transition movement and the model motion might exist for a given frequency stated in [10] cannot be confirmed by the results of this work. The only frequency reaching a nearly constant time delay is the lowest frequency investigated because the flow is close to steady conditions, as shown in Fig. 14. A really constant time delay is probably only existing for the borderline case with $k = 0$, and in this case the time delay is zero since it is the steady case.

6 CONCLUSIONS

The unsteady boundary layer transition on the pitching rotor blade airfoil DSA-9A was experimentally investigated at $M = 0.30$ and $Re = 1.8 \times 10^6$ by the use of hot film anemometry and high speed pressure measurements. Results were presented for the upper and the lower side of the airfoil for a static polar and dynamic test cases with sinusoidal pitching motion in attached flow conditions. Automated transition detection was applied, allowing the detailed analysis of the onset and the end of the transition zone as well as of 50% intermittency.

The results showed that a significant transition movement exists on both sides of the airfoil for a motion of $\alpha = 4^\circ \pm 6^\circ$ and $k = 0.060$. On the upper side, a slow continuous movement of the transition occurs, which is in qualitative agreement with the results of other researchers. A much faster and rather discontinuous movement in the

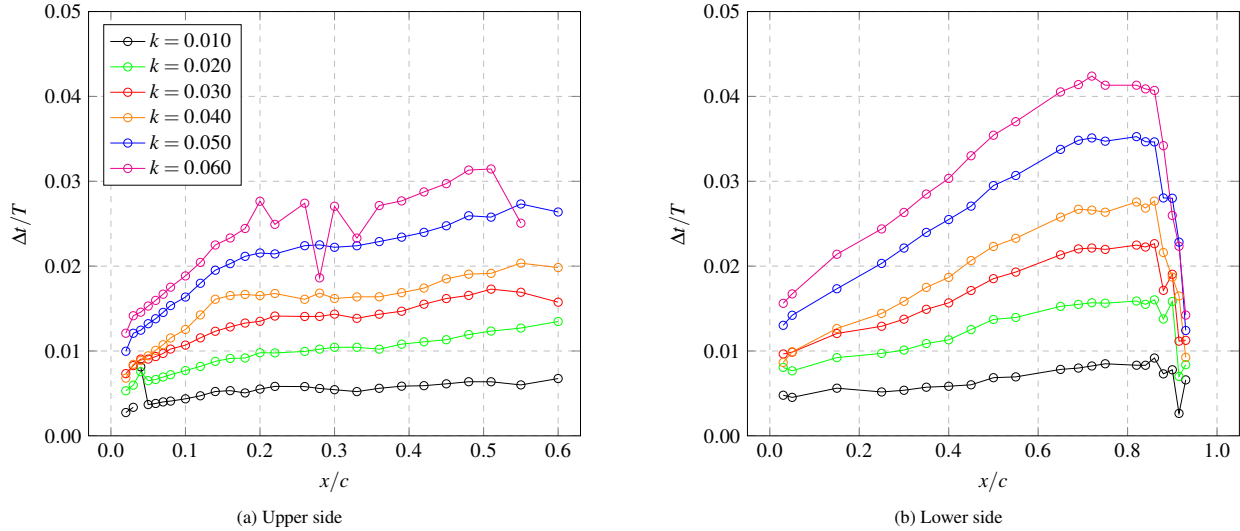


Figure 17: Frequency effect on the time delay between between 50% intermittency and the model motion for $\alpha = 5^\circ \pm 7^\circ$, $M = 0.30$, and $Re = 1.8 \times 10^6$

opposite direction exists over the entire lower side, providing laminar flow upstream of the tab during a large part of the pitching cycle. A significant hysteresis between the upstroke and the downstroke transition locations exists on both sides that are each much larger than the hysteresis in lift. The steady transition behavior lies within the unsteady hysteresis but no consistent trend could be identified.

Significant transition zones exist on the airfoil with varying sizes depending on the angle of attack or the onset position of the transition. Small zones appear near the leading edge and the length increases downstream. On the lower side, much larger transition zones (up to 55% chord) than on the upper side (up to 20% chord) occur and a strong effect of the direction of the pitching motion was found. Compared to the steady conditions, slightly larger zones exist on the pitching airfoil.

Due to the movement of the transition zones over the airfoil, different positions on the airfoil are exposed to intermittent flow for varying time spans. In general, the time spans are in the same order of magnitude on the largest part of both airfoil sides and reach up to 13% of the cycle. In the trailing edge region of the lower side, however, time spans of up to 50% of the cycle occur. The time spans were found to depend on the relative motion between the transition movement and the flow. The time spans are smaller, i.e. the transition moves faster, when the transition moves against the main flow direction.

An assessment of the unsteadiness of the transition movement revealed that the movement on the upper side is quasi-steady, whereas a real unsteady behavior is seen on the lower side. On the upper side, the transition zone is estimated to shift by less than 1% chord during a fluid element passes the zone, while up to 13% chord are reached on the lower side.

The influence of the variation of the pitching frequency

for $\alpha = 5^\circ \pm 7^\circ$ from $k = 0.010$ to $k = 0.060$ was seen in a significant increase in the hysteresis between the upstroke and the downstroke. Both the onset and the end of transition are shifted to higher angles of attack during the upstroke, and to lower angles of attack during the downstroke. The effect is larger on the lower side than on the upper side, is different between the onset and the end of the transition, and depends on the upstroke/downstroke motion.

The size of the transition zone mainly reduces with increasing pitching frequency, and a similar effect was found for the period of intermittent flow during the pitching cycle. The time delay between the transition movement and the model motion increases with the pitching frequency, and depends on the chordwise position and the upstroke/downstroke motion.

ACKNOWLEDGMENTS

The authors are grateful for the assistance of several colleagues of the DLR Institute of Aeroelasticity, the German-Dutch Wind Tunnels, the DLR Workshops and the DLR Institute of Aerodynamics and Flow Technology.

REFERENCES

- [1] Y. Sémézis, P. Beaumier, “Determination de l’état de la couche limite sur des sections de pale d’hélicoptère à l’aide de films chauds”, Technical report ONERA-TAP-95-065, ONERA Chatillon, 1995.
- [2] M. Raffel, E. de Gregorio, K. de Groot, O. Schneider, G. Gibertini, A. Seraudie, “On the Generation of a Helicopter Aerodynamic Database”, *The Aeronautical Journal*, Vol. 115, No. 1164, 2011, pp. 103–112.
- [3] J. de Ruyck, B. Hazarika, Ch. Hirsch, “Transition and Turbulence Structure in the Boundary Layers of an

Oscillating Airfoil”, Vrije Universiteit Brussel, Research report VUB-STR-16, 1989.

- [4] S. Schreck, W. Faller, H. Helin, “Pitch Rate and Reynolds Number Effects on Unsteady Boundary Layer Transition and Separation”, *Journal of Aircraft*, Vol. 35, No. 1, 1998, pp. 46–52, DOI: 10.2514/2.2258.
- [5] M. Pascazio, J. Autric, D. Favier, C. Maresca, “Unsteady boundary-layer measurement on oscillating airfoils – Transition and separation phenomena in pitching motion”, 34th AIAA Aerospace Sciences Meeting and Exhibit, Reno, NV, January 15–18, 1996, DOI: 10.2514/6.1996-35.
- [6] T. Lee, S. Basu, “Measurement of Unsteady Boundary Layer Developed on an Oscillating Airfoil Using Multiple Hot-Film Sensors”, *Experiments in Fluids*, Vol. 25, No. 2, 1998, pp. 108–117.
- [7] T. Lee, P. Gerontakos, “Investigation of Flow Over an Oscillating Airfoil”, *Journal of Fluid Mechanics*, Vol. 512, 2004, pp. 313–341, DOI: 10.1017/S0022112004009851.
- [8] P. Lorber, F. Carta, “Unsteady Transition Measurements on a Pitching Three-Dimensional Wing”, 5th Symposium on Numerical and Physical Aspects of Aerodynamic Flows, Long Beach, CA, January 13–15, 1992.
- [9] M. S. Chandrasekhara, M. C. Wilder, “Heatflux Gauge Studies of Compressible Dynamic Stall”, *AIAA Journal*, Vol. 41, No. 5, 2003, pp. 757–762, DOI: 10.2514/2.2019.
- [10] K. Richter, S. Koch, A. D. Gardner, “Influence of oscillation amplitude and Mach number on the unsteady transition on a pitching rotor blade airfoil”, American Helicopter Society 69th Annual Forum, Phoenix, Arizona, May 21-23, 2013.
- [11] K. Richter, S. Koch, A. D. Gardner, H. Mai, A. Klein, C.-H. Rohardt, “Experimental investigation of unsteady transition on a pitching rotor blade airfoil”, *Journal of the American Helicopter Society*, Vol. 59, No. 1, 2014, DOI: 10.4050/JAHS.59.012001.
- [12] M. Tiedemann, “Investigation of the unsteady rotor boundary layer transition in a transonic high pressure turbine stage”, DLR report DLR-FB–98-30, 1998.
- [13] V. A. Tet’anko, “Coefficient of skewness in the distribution of velocity fluctuations in laminar-turbulent boundary layer transition”, *Journal of Applied Mechanics and Technical Physics*, Vol. 22, No. 5, 1981, pp. 683–685, DOI: 10.1007/BF00913721.
- [14] H. Schlichting, K. Gersten, “Boundary-layer theory”, In: 8th revised and enlarged edition, Springer, Berlin, ISBN 3-540-66270-7, 2000.
- [15] W. Johnson, “A History of Rotorcraft Comprehensive Analyses”, NASA-TP-2012-216012, 2012.
- [16] T. Theodorsen, “General Theory of Aerodynamic Instability and the Mechanism of Flutter”, NACA-TR-496, 1934.